AGU PUBLICATIONS

Geochemistry, Geophysics, Geosystems

RESEARCH ARTICLE
10.1002/2014GC005386

Special Section:
Magnetism From Atomic to Planetary Scales: Physical Principles and Interdisciplinary Applications in Geo- and Planetary Sciences

Key Points:
- The maximum susceptibility in fresh olivine with >3wt % FeO is parallel to *c*
- At RT the minimum susceptibility lies along *a* or *b* depending on the Fe content
- At 77 K the minimum susceptibility is parallel to the crystal's *b* axis

Supporting Information:
- Readme
- Figures a and b
- Tables a-c

Correspondence to:
A. M. Hirt,
ann.hirt@erdw.ethz.ch

Citation:
Biedermann, A. R., T. Pettke, E. Reusser, and A. M. Hirt (2014), Anisotropy of magnetic susceptibility in natural olivine single crystals, *Geochem. Geophys. Geosyst.*, *15*, 3051–3065, doi:10.1002/2014GC005386.

Received 18 APR 2014
Accepted 9 JUL 2014
Accepted article online 12 JUL 2014
Published online 31 JUL 2014

Anisotropy of magnetic susceptibility in natural olivine single crystals

Andrea R. Biedermann[1], Thomas Pettke[2], Eric Reusser[3], and Ann M. Hirt[1]

[1]Institute of Geophysics, ETH Zurich, Zurich, Switzerland, [2]Institute of Geological Sciences, University of Bern, Bern, Switzerland, [3]Institute of Geochemistry and Petrology, ETH Zurich, Zurich, Switzerland

Abstract Mantle flow dynamics can cause preferential alignment of olivine crystals that results in anisotropy of physical properties. To interpret anisotropy in mantle rocks, it is necessary to understand the anisotropy of olivine single crystals. We determined anisotropy of magnetic susceptibility (AMS) for natural olivine crystals. High-field AMS allows for the isolation of the anisotropy due to olivine alone. The orientations of the principal susceptibility axes are related to the olivine's crystallographic structure as soon as it contains >3 wt % FeO. The maximum susceptibility is parallel to the *c* axis both at room temperature (RT) and at 77 K. The orientation of the minimum axis at RT depends on iron content; it is generally parallel to the *a* axis in crystals with 3–5 wt % FeO, and along *b* in samples with 6–10 wt % FeO. The AMS ellipsoid is prolate and the standard deviatoric susceptibility, k', is on the order of $8*10^{-10}$ m^3/kg for the samples with <1wt % FeO, and ranges from $3.1*10^{-9}$ m^3/kg to $5.7*10^{-9}$ m^3/kg for samples with 3–10 wt % FeO. At 77 K, the minimum susceptibility is along *b*, independent of iron content. The shape of the AMS ellipsoid is prolate for samples with <5 wt % FeO, but can be prolate or oblate for higher iron content. The degree of anisotropy increases at 77 K with $p'_{77} = 7.1 \pm 0.5$. The results from this study will allow AMS fabrics to be used as a proxy for olivine texture in ultramafic rocks with high olivine content.

1. Introduction

Olivine is one of the most common minerals on Earth, constituting a large fraction of the Earth's upper mantle. Other terrestrial planets (Mercury, Venus, or Mars) are also thought to have high concentration of olivine in their upper mantle. Olivine is also abundant in meteorites and contains inclusions of ferromagnetic minerals, which are capable of acquiring a remanent magnetization. Therefore, there has been interest in using olivine as a recorder of the extraterrestrial magnetic field [*Hoffmann et al*., 2011; *Lappe et al*., 2011; *Rochette et al*., 2009; *Uehara and Nakamura*, 2006]. On Earth, the rheology of olivine determines flow dynamics in depths shallower than 410 km; thus, olivine properties influence mantle flow and plate tectonics. Plastic flow causes a preferred orientation of olivine crystals, which is responsible, for example, for seismic anisotropy in the upper mantle [e.g., *Nicolas and Christensen*, 1987; *Silver*, 1996]. The crystallographic preferred orientation of olivine grains in peridotite bodies has been used to define flow dynamics in the upper mantle or detect lithospheric deformation [e.g., *Hrouda et al*., 2009]. In addition, olivine texture can influence the location and orientation of deformation zones, because anisotropic viscosity causes a localization of shear stresses [*Tommasi et al*., 2009]. These deformation zones can evolve into future plate boundaries.

Anisotropy of magnetic susceptibility (AMS) is commonly used as an indicator of the texture of a rock. The AMS of a whole rock consists of a superposition of diamagnetic and paramagnetic components which can be linked to silicate or carbonate minerals, and ferromagnetic components, which are associated with iron oxides, hydroxides, or sulfides as inclusions or separate grains. Diamagnetic anisotropy is often negligible in rocks that contain iron-bearing minerals. Paramagnetic anisotropy, however, can be significant and arises principally from the distribution of iron ions in the crystal lattice. Consequently, magnetic anisotropy arising from paramagnetic minerals can be used to determine the crystallographic orientations of these minerals in a rock. To fully interpret the paramagnetic AMS, the single-crystal properties of all the minerals in a rock must be known.

Only a few studies have been made on the magnetic anisotropy of natural olivine and have yielded inconsistent results [*Belley et al*., 2009; *Ferré et al*., 2005a, b], and a summary is given below. To resolve these inconsistencies in the literature, we conduct a thorough study of the magnetic anisotropy of olivine,

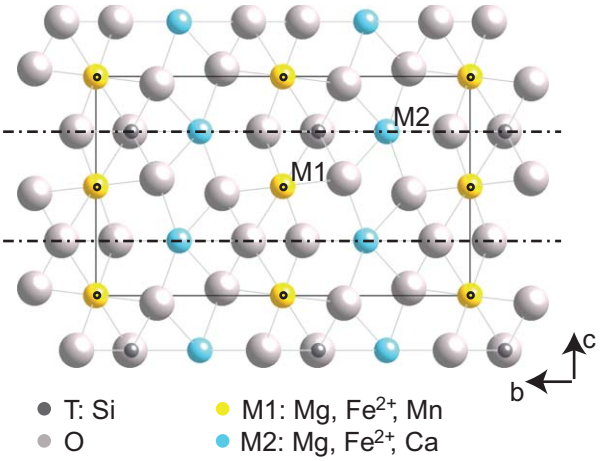

Figure 1. Olivine crystal structure, view along the *a* axis. Oxygen and silicon atoms form tetrahedra, which are linked by magnesium or iron ions that can occupy either M1 or M2 sites. M1 sites represent inversion centers (o), whereas M2 sites lie on mirror planes (--).

addressing the crystal chemistry, paramagnetic and ferromagnetic contributions to the AMS, and the relation of magnetic anisotropy to the crystallographic lattice structure. We examine both low-field and high-field AMS in 35 olivine single crystals, focusing on natural samples, which are most relevant to mantle deformation models. The main goal of this study is to define the single-crystal AMS of pure olivine and to understand how it varies with chemical composition. Because magnetic anisotropy is easily determined, allowing evaluation of a large number of samples, it can be used as a first-order proxy for texture in mantle rocks, therefore mantle flow. Based on our results, it will be possible to obtain insight into the rock texture from AMS measurements, which are fast and easy to perform. This will have implications on fabric as well as geodynamic studies. Because magnetic anisotropy can serve as a first-order proxy for texture in mantle-derived rocks, it will also provide information on the relative degree of seismic anisotropy.

2. Geophysical Background

The olivine group includes the minerals olivine, forming a continuous solid solution series between forsterite (Mg_2SiO_4) and fayalite (Fe_2SiO_4), tephroite (Mn_2SiO_4), knebelite ($(Mn,Fe)_2SiO_4$), and monticellite ($Ca(Mg,Fe)SiO_4$) [*Deer et al.*, 1997]. Various members of the forsterite-fayalite solid solution series are considered in this study, referred to as olivine. Tephroite, knebelite, and monticellite are subordinate on Earth. Mg-rich olivine dominates in the Earth's upper mantle and is a common rock-forming mineral, especially in ultramafic rocks [e.g., *Deer et al.*, 1997]. Olivine is an orthorhombic crystal with space group *Pbnm*. Its structure consists of isolated $(SiO_4)^{4-}$ tetrahedra, which are linked mainly by Mg^{2+} or Fe^{2+} ions in octahedral coordination. Other cations are almost exclusively divalent; if trivalent cations are present, they occur in very small amounts. There are two types of distorted octahedral sites, labeled M1 and M2, which have different symmetry: M1 sites represent centers of symmetry, whereas M2 sites lie on mirror planes (Figure 1).

Magnetic susceptibility is an intrinsic property of a material, relating the magnetization induced by an applied magnetic field to the strength of the field. Susceptibility anisotropy can be described by a second-order tensor. This tensor is symmetric and can be represented by an ellipsoid whose principal axes ($k_1 \geq k_2 \geq k_3$) correspond to the eigenvalues of the tensor. AMS can be described by a full tensor, whose elements are full directional values of the susceptibility, or by a deviatoric tensor, whose elements are the differences in susceptibility from the mean susceptibility. The magnetic susceptibility ellipsoid is generally characterized by its degree of anisotropy and shape and the directions of the principal axes. Because we use a method to isolate the paramagnetic anisotropy, which only gives the deviatoric susceptibility, the degree of anisotropy is defined by the standard deviatoric susceptibility, k' [*Jelinek*, 1984].

$$k' = \sqrt{\frac{(k_1-k)^2+(k_2-k)^2+(k_3-k)^2}{3}}$$

where k is the mean susceptibility. The shape of the AMS ellipsoid is defined by U [*Jelinek*, 1981]

$$U=(2k_2-k_1-k_3)/(k_1-k_3)$$

U is between 0 and +1 for an oblate ellipsoid, between 0 and −1 for a prolate ellipsoid and close to 0 for a neutral ellipsoid.

The paramagnetic component of the susceptibility and its anisotropy vary with temperature according to the Curie-Weiss law; the paramagnetic susceptibility becomes enhanced with decreasing temperature and both the AMS degree and shape can vary as a function of temperature.

AMS of a bulk rock is often used as a proxy for mineral fabric or deformation. For example, *Ferré et al*. [2005b] found that the paramagnetic component of the high-field anisotropy in mantle peridotite can be related to the lattice-preferred orientation of olivine. In order to understand this relationship, however, it is essential to know the single-crystal anisotropies of the minerals composing the rock. In the case of mantle peridotite, this is Mg-rich olivine.

Olivine often contains inclusions, such as iron-bearing oxides, sulfides, or silicate melt. Magnetite is a common ferrimagnetic mineral in mantle rocks. Developing at high temperature in an olivine grain, magnetite often forms rods or lamellae in specific directions in the olivine lattice. Magnetite in a rock can oxidize to hematite upon weathering and in olivine hematite mainly occurs as diffusion rims along grain boundaries, thus indicating its secondary origin [e.g., *Deer et al*., 1997]. Iron sulphides, e.g. pyrrhotite, are also known to occur as melt inclusions or grains in mantle rocks. In order to eliminate any contributions from ferromagnetic (*s.l.*) inclusions to the magnetic anisotropy, the paramagnetic component, which depends on the silicate structure, must be isolated. This paramagnetic fabric can be related to the mineral fabric in the mantle. It is not possible to separate the paramagnetic anisotropy when measuring low-field susceptibility. Because paramagnetism is linearly related to the strength of the applied field, whereas ferrimagnetic minerals will be saturated in fields $<$600 mT, it is possible to separate the anisotropic component due to paramagnetic minerals from that of saturated ferrimagnetic minerals [e.g., *Hrouda*, 1982; *Owens and Bamford*, 1976]. Thus, the paramagnetic anisotropy can be related to the olivine lattice.

The bulk susceptibility of olivine with various compositions was investigated first by *Nagata et al*. [1957]. They attributed the paramagnetic susceptibility of olivine to Fe^{2+} ions in the crystal structure and found a linear relationship between molar susceptibility and fayalite content x_{fa}:

$$\chi_{mol,olivine} = 2.2^{*}10^{-2}x_{fa} \quad \text{to} \quad 2.6^{*}10^{-2}x_{fa} \ \ emu/mol.$$

Later work by *Hoye and O'Reilly* [1972] and *Belley et al*. [2009] in natural and synthetic crystals or synthetic powders covered the complete compositional range between the forsterite and fayalite end-members. *Hoye and O'Reilly* [1972] calculated olivine mass susceptibility based on

$$\chi = \frac{2p_{eff}^2 \mu_B^2 xN}{3k_b M_x (T-\theta)}$$

where $p_{eff}=5.2$ is the effective number of Bohr magnetons (μ_B) per iron atom, x the fayalite mole fraction, N Avogadro's number, k_b Boltzmann's constant, and M_x the molar weight of a crystal with fayalite content x, T is the measurement temperature, and θ the ordering temperature. They reported higher susceptibilities than predicted by Nagata's formula. *Belley et al*. [2009] found $p_{eff} = 6.03$.

Several studies have examined the magnetic anisotropy in synthetic fayalite, Fe_2SiO_4 [*Ballet et al*., 1989; *Cococcioni et al*., 2003; *Ehrenberg and Fuess*, 1993; *Müller et al*., 1982], and $(Fe,Mn)_2SiO_4$ [*Ballet et al*., 1987]. Fayalite has been reported to undergo antiferromagnetic ordering below 64.9 K, whereby the magnetic moments on the M2 sites are parallel to the crystallographic *b* axis, whereas those on M1 sites are canted [*Ehrenberg and Fuess*, 1993]. The canting angle decreases with temperature. The maximum susceptibility of fayalite is parallel to the *c* axis, independent of temperature. Below the Néel temperature, the susceptibility anisotropy is clearly triaxial, with k_3 aligning with the *b* axis. At room temperature, however, the anisotropy is uniaxial with nearly equal susceptibilities parallel to the crystallographic *a*- and *b*-axes of fayalite [*Ballet et al*., 1989; *Ehrenberg and Fuess*, 1993; *Müller et al*., 1982]. In its ground state, spins are coupled antiferromagnetically between corner-sharing octahedra and ferromagnetically between edge-sharing octahedra [*Cococcioni et al*., 2003; *Müller et al*., 1982]. *Ballet et al*. [1987] concluded that the ionic anisotropy of Fe^{2+} is responsible for the crystal anisotropy and that the easy direction of magnetization depends on the relative distribution of Fe^{2+} on M1 and M2 sites. If Fe^{2+} is primarily located on M1 sites, the easy magnetization direction is parallel to the crystallographic *c* axis, whereas it is parallel to *b* when Fe^{2+} is concentrated on M2 sites.

Belley et al. [2009] investigated the AMS of four olivine crystals with composition close to forsterite and found that the maximum susceptibility was parallel to *a*, and the minimum susceptibility parallel to *b*. They

Table 1. Sample Locations, Sample Masses, and Forsterite and Fayalite Contents

Sample	Mass (g)	Location	Comment	MgO wt %	FeO wt %	x_{Mg}	x_{Fe}
Fo1	0.45	Burma		57.3	1.0	99.1	0.9
Fo2	0.40	Burma		57.3	1.0	99.1	0.9
NMB14203	0.60	Zabargad Island, Red Sea, Egypt		50.9	8.7	91.2	8.8
NMB28855	0.43	Arizona, US		52.5	7.4	92.6	7.4
NMB45445	6.07	Sapat Complex, Kohistan, Pakistan	Needles of dark inclusions	54.1	3.8	96.2	3.8
NMB47213	3.05	Sapat Complex, Kohistan, Pakistan		52.9	4.7	95.3	4.7
Ol1	1.78	Sapat Complex, Kohistan, Pakistan		53.9	3.7	96.2	3.8
Ol2	2.98	Unknown		53.0	7.7	92.5	7.5
Ol3	1.12	Unknown		50.1	7.6	92.2	7.8
Ol9	0.20	China		58.4	8.1	92.8	7.2
Ol10	0.13	China		57.4	8.3	92.5	7.5
Ol11	0.09	China		50.8	8.2	91.7	8.3
Ol12	0.15	China		58.2	8.1	92.8	7.2
Ol14	0.72	Sapat Complex, Kohistan, Pakistan	Spherical dark inclusions	52.1	7.6	92.4	7.6
Ol15	0.28	Sapat Complex, Kohistan, Pakistan		51.8	7.6	92.4	7.6
Ol16	2.11	San Carlos Olivine[a]		49.4	9.6	90.2	9.8
Ol17	2.73	San Carlos Olivine[a]		49.4	9.6	90.2	9.8
Ol18	2.41	San Carlos Olivine[a]		49.4	9.6	90.2	9.8
Ol19	3.64	San Carlos Olivine[a]		49.4	9.6	90.2	9.8
Ol20	2.95	San Carlos Olivine[a]		49.4	9.6	90.2	9.8
Ol21	2.71	San Carlos Olivine[a]		49.4	9.6	90.2	9.8
Ol22	2.63	San Carlos Olivine[a]		49.4	9.6	90.2	9.8
Ol23	0.99	Sapat Complex, Kohistan, Pakistan		53.5	4.2	95.7	4.3
Ol24	3.55	Sapat Complex, Kohistan, Pakistan		54.3	4.2	95.8	4.2
Ol25	1.41	Sapat Complex, Kohistan, Pakistan		51.7	8.4	91.6	8.4
Ol26	1.31	Sapat Complex, Kohistan, Pakistan		56.3	4.6	95.6	4.4
Ol27	1.70	Sapat Complex, Kohistan, Pakistan		54.6	4.1	96.0	4.0
Ol28	1.60	Sapat Complex, Kohistan, Pakistan		53.6	3.8	96.1	3.9
Ol29	2.49	Sapat Complex, Kohistan, Pakistan		54.0	4.0	96.0	4.0
Ol30	2.22	Sapat Complex, Kohistan, Pakistan		49.2	6.6	93.0	7.0
Ol31	1.16	Sapat Complex, Kohistan, Pakistan		53.0	4.6	95.4	4.6
Ol32	0.41	Tanzania	Strongly weathered	43.2	16.9	82.0	18.0
Ol33	0.40	Tanzania	Strongly weathered	43.1	16.7	82.1	17.9
Ol34	0.54	Tanzania	Strongly weathered	43.3	16.8	82.2	17.8
Ol35	0.81	Tanzania	Strongly weathered	42.9	17.0	81.8	18.2

[a]Compositional parameters for San Carlos Olivine were taken from *Jarosewich et al.* [1980].

attributed the disagreement with the fayalite studies to the different chemical composition. *Ferré et al.* [2005b] measured one crystal with forsterite composition and found a maximum susceptibility along *c*, and minimum susceptibility along *b*. The authors corrected this original finding to a maximum susceptibility parallel to *a*, and minimum parallel to *c* [*Ferré et al.*, 2005a].

3. Methods

3.1. Sample Description

A collection of 35 natural olivine single crystals were investigated (Table 1). Samples were borrowed from the Natural History Museum Basel (labeled NMB), the Mineral Collection of ETH Zurich, Durham University, the Swiss Gemmological Institute, or collected during fieldwork. The samples are from different geological environments and cover the compositional range from $x_{Mg} = 0.82$ to 0.99. Seven crystals (Ol16–Ol22) are San Carlos olivine, extracted from peridotite xenoliths, which are often used as reference crystals. Four crystals were extracted from a peridotite xenolith in Cenozoic basalt from the Hannuoba area in the North China craton (Ol9–Ol12). These xenoliths contain coarse- to medium-grained spinel lherzolite and are described by *Chen et al.* [2001] and *Rudnick et al.* [2004]. The two forsterite specimens (Fo1, Fo2) originate from a skarn in Burma. Samples Ol1, Ol14, Ol15, Ol23–Ol31, NMB45445, and NMB47213 are gem-quality crystals from the Sapat mafic-ultramafic complex, Pakistan [*Kane*, 2004]. There, the gem-olivine occurs in fluid-derived veins in the dunite that represents the arc mantle of the Kohistan arc [*Bouilhol et al.*, 2009, 2012]. A similar genetic type of olivine (NMB14203) is found on Zabargad Island, Egypt, which is also known for its gem-quality olivine. Here, olivinite veins cut ultramafic bodies, representing fertile upper mantle material, such as spinel

and spinel-plagioclase lherzolite [*Kurat et al*., 1993]. Another sample (NMB28855) comes from Arizona, US; its exact location, however, is not known. Samples Ol2 and Ol3 also come from unknown locations. Four samples (Ol32–Ol35) were collected south of Oldoinyo Lengai, Tanzania. These crystals are strongly weathered and exhibit a brown color typical for iddingsitation.

3.2. Chemical Composition

In order to correlate magnetic properties of olivine with their chemistry, the *bulk* sample chemical composition is required, because inclusions, whether they are submicroscopic or microscopic, can affect magnetization parameters. Compositional data were therefore acquired for most samples by laser ablation inductively coupled plasma mass spectrometry (LA-ICP-MS) at the Institute of Geological Sciences, University of Bern. Details of instrumental setup and optimization strategies are reported elsewhere [*Pettke et al*., 2012]. LA-ICP-MS was preferred to conventionally employed electron probe microanalysis (EPMA), because LA-ICP-MS allows analysis of a larger sample volume than that analyzed by EPMA. In this way, the average composition of a large sample can be determined accurately with fewer spot measurements than would be required for EPMA, while maintaining analytical resolution to identify crystal-chemical zoning at the 100 μm scale. It should be noted, however, that analytical accuracy for major element composition is inferior for LA-ICP-MS (1–2% 2SD) relative to that typical of EPMA. A 120 μm wide beam was used with LA-ICP-MS and at least four spots were measured per crystal to investigate chemical homogeneity. Element concentration data were calculated assuming that the total of major oxides is 100 wt % and that iron is present exclusively as Fe^{2+}. Data processing was performed using SILLS [*Guillong et al*., 2008].

Chemical analysis of the gemstone quality crystals Ol23–Ol31 was performed using EPMA, because no destructive measurements were possible on these samples [cf. *Bouilhol et al*., 2012, for ICP-MS analyses of samples from the Sapat complex]. Each crystal was wrapped in aluminum foil prior to measurement. A hole was cut into the foil above the best natural surface of the crystal and a drop of silver served as conductor. The analyses were made on a JEOL JXA-8200 electron microprobe at the Institute of Geochemistry and Petrology, ETH Zurich. The instrument was operated at an accelerating voltage of 15 kV, a beam current of 20 nA and with a focused beam. Synthetic forsterite and fayalite and synthetic and natural oxides were used as standards. Several spots have been measured to check for sample homogeneity. The data were φ-ρ-z corrected.

3.3. Magnetic Measurements

Accurate crystallographic orientation of samples is mandatory for relating magnetic anisotropy to crystal structure. The orientation of each single crystal was determined by Laue X-ray diffraction measured at the Laboratory of Crystallography, ETH Zurich. The X-rays were generated in a Mo-tube operated at 50 kV and 35 mA. The Laue photographs were acquired in reflection mode with 4 min exposure time. Data analysis was performed using the OrientExpress orientation software [*Laugier and Filhol*, 1983]. With this method, crystals could be oriented to an accuracy of ± 2 degrees. All magnetic measurements were made at the Laboratory of Natural Magnetism, ETH Zurich.

3.3.1. Acquisition of Isothermal Remanent Magnetization (IRM) and Hysteresis Properties

Acquisition of IRM was used to identify ferromagnetic inclusions in the olivine crystals. For this purpose, the sample was magnetized with a pulse magnetizer (ASC Scientific, IM-10-30) in a field of 2 T in a known direction. Then, the sample was remagnetized in progressively higher fields in the opposite direction. After each applied field, the magnetization was measured with a 2G Enterprises cryogenic magnetometer (Model 755). The saturation remanent magnetization (SIRM) and remanent coercivity indicate the relative concentration and type of ferromagnetic grains in the sample.

Hysteresis curves were measured on selected samples on a Princeton Measurements Corporation MicroMag 3900 vibrating sample magnetometer (VSM) in fields up to 1 T to further help identify the ferromagnetic minerals, based on their coercivity and saturation magnetization. Magnetization curves were obtained using mixed increments of 10 mT between 100 mT and 1000 mT, 1 mT between 20 mT and 100 mT and 0.5 mT for applied fields lower than 20 mT. The slope of the high-field hysteresis curve was used as an independent estimate of the paramagnetic susceptibility.

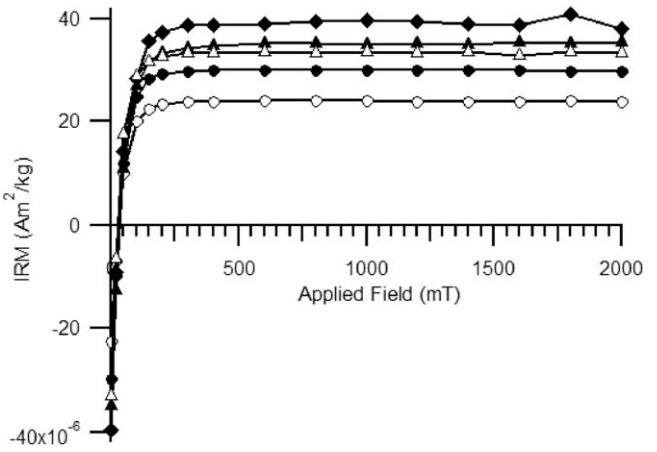

Figure 2. Representative IRM acquisition curves show low coercivities and saturation fields for the ferromagnetic inclusions.

3.3.2. Low-Temperature Magnetization Curves

Low-temperature magnetization curves were measured on two crystals on which destructive measurements were allowed. Magnetization parallel to each of the crystallographic axes was measured on a Quantum Design Magnetic Property Measurement System (MPMS) at the Laboratory for Solid State Physics, ETH Zurich. The temperature dependence of the susceptibility was measured in fields of 1 T and 0.01 T and for a temperature range between 300 and 2 K. The cooling rate was 10 K/min and the temperature was stabilized prior to each susceptibility measurement.

3.3.3. Anisotropy of Magnetic Susceptibility

Anisotropy of magnetic susceptibility was measured in low and high magnetic fields. The sum of the diamagnetic, paramagnetic and ferromagnetic contributions of all mineral grains in the sample is measured with both instruments. Low-field AMS was determined with an AGICO MFK1-FA Kappabridge in a magnetic field of 200 A/m and with a frequency of 976 Hz. Weak samples were remeasured in 500 A/m fields. The susceptibility tensor was calculated from 15 directional measurements. In order to increase data quality, the values for 10 measurements in each direction were stacked [*Biedermann et al*., 2013].

High-field AMS was measured on a torque magnetometer in six different fields between 1.0 T and 1.5 T [*Bergmüller et al*., 1994]. Measurements were obtained in three mutually perpendicular planes, using a 30° measurement increment in each plane. The torque magnetometer determines the deviatoric susceptibility tensor. High-field measurements were conducted both at room temperature and at 77 K. The fields, which were applied, are large enough to saturate magnetite inclusions. When saturated, the ferromagnetic contribution to the torque signal is independent of any increase in the field, whereas the paramagnetic contribution increases in proportion to the square of the field. This allows for separation of the diamagnetic, paramagnetic, and ferrimagnetic contributions to the high-field AMS [*Martín-Hernández and Hirt*, 2001, 2004; *Schmidt et al*., 2007].

4. Results

4.1. Chemical Composition

The olivine sample suite covers the compositional range from Fo90 to Fo99 for the fresh samples and Fo82 for the strongly weathered olivines (Table 1, and supporting information, Table A). Low spot-to-spot variability of most elements indicates that cations are homogeneously distributed within most crystals. There are several exceptions, such as for NMB45445, which exhibits macroscopically visible dark needle-shaped inclusions. According to *Bouilhol et al*. [2012], needles of Mg-Fe borates are characteristic for Sapat olivine. Sample Ol14 comprises spherical black inclusions that may correspond to magnetite. Additionally, Ol2 and NMB28855 contain melt inclusions characterized by elevated bulk contents of Fe and high concentrations of rare earth elements. In the fresh samples, the Ni content varies between 1900 and 3000 μg/g. Other cations with large magnetic moments, such as Cr or Mn, are only present in very small amounts ($<$1 wt % MnO; $<$ 300 μg/g Cr). The weathered samples from Tanzania have different compositions, with higher iron contents, and larger amounts of other elements such as Ti, Mn, Ca, Na, K, Zn, Sr, and Zr, compared to fresh olivine. Their Ni content varies between 1000 and 1100 μg/g and Cr is ∼60 μg/g.

Table 2. Saturation Remanence and its Effect on Susceptibility

Sample	SIRM (Am^2/kg)	Influence on LF AMS Directions	Influence on k_{mean}
NMB14203	5.39E-05	None	None
NMB28855	6.99E-05	Tilt of k_1, k_2	None
NMB45445	1.08E-03	All axes tilted	Yes
NMB47213	1.17E-04	Tilt of k_1, k_3	None
Ol1	7.11E-05	Tilt of k_2, k_3	None
Ol2	3.59E-05	None	None
Ol3	3.10E-05	None	None
Ol9	1.08E-04	Tilt of k_1, k_2	None
Ol10	1.79E-04	Tilt of k_1, k_2	None
Ol12	1.13E-04	Tilt of k_1, k_2	None
Ol14	3.74E-03	All axes tilted	Yes
Ol15	1.14E-04	None	None
Ol16	1.80E-05	None	None
Ol22	1.49E-05	None	None
Ol27	8.68E-05	None	None
Ol30	7.14E-04	None	Yes
Ol31	1.05E-04	None	None
Ol34	7.72E-03	All axes tilted	Yes
Ol35	2.13E-03	All axes tilted	Yes

4.2. IRM Acquisition and Hysteresis

The acquisition of IRM was measured on selected crystals from the different localities (Figure 2). All samples have a remanent coercivity $<$50 mT, and samples NMB45445, Ol14, and Ol31 have a coercivity value $<$20 mT. Samples NMB45445 and NMB47213, Ol14 and Ol15 saturate in fields below 200 mT, while the remaining crystals are saturated by 300 mT. NMB45445, Ol14, Ol34, and Ol35 have the strongest saturation magnetizations indicating the highest concentrations of ferromagnetic inclusions (Table 2). It should be noted that saturation is reached well below 1 T, which allows for a reliable separation of paramagnetic and ferromagnetic contributions using high-field AMS.

Hysteresis was measured on the samples small enough to fit in-between the poles of the vibrating sample magnetometer. Many samples showed a positive linear relationship between field and magnetization, which indicates the presence of only a paramagnetic component. Those samples with a ferromagnetic (*s.l.*) contribution showed low coercivities and were magnetically saturated by 300 mT. Because the cryogenic magnetometer is more sensitive in detecting remanent magnetization than the VSM, magnetite was identified in Ol2 and Ol3 from IRM acquisition, whereas the hysteresis curves show a pure paramagnetic component.

4.3. Magnetic Susceptibility and Anisotropy

4.3.1. Low-Temperature Susceptibility

Low-temperature susceptibility was determined for Ol14 and Ol15. The measurements show that the increase in directional susceptibility with decreasing temperature is anisotropic. For temperatures larger than ~100 K, the susceptibility can be approximated by a Curie-Weiss law along all three crystallographic axes:

$$\chi_{obs} = \frac{M}{H} = \mu_0 \frac{C}{T-\theta} + \chi_0$$

where χ_{obs} is the molar susceptibility, M the measured magnetization in the applied field H, μ_0 the permeability of free space, C the Curie constant, and χ_0 a temperature-independent background, such as diamagnetic or van Vleck paramagnetic susceptibility. The Curie constant is defined as:

$$C = \frac{\mu_B{}^2 g^2 S(S+1)N}{3k_b}$$

Table 3. Paramagnetic Curie Temperatures and g-Factors Obtained from Low-Temperature Susceptibility Curves of Ol14 and Ol15

Field Direction	g (−)	θ (K)	χ_0 (m^3/mol)
Ol14			
H//a	1.85	−11	9.7E-10
H//b	1.91	−18	−4.5E-11
H//c	1.86	−4	1.8E-09
Ol15			
H//a	2.12	−11	2.8E-09
H//b	2.18	−18	1.4E-09
H//c	2.16	−6	2.4E-09

where μ_B is the Bohr magneton, g is Landé's g-factor, S is the spin number, N is the number of magnetic ions, and k_b is Boltzmann's constant. Ferrous iron possesses a spin $S = 2$. The material constants g and θ depend on the crystallographic direction as shown in Table 3.

Local magnetic ordering sets in below approximately 100 K when the field is parallel to *b*, resulting in a smaller increase in the susceptibility than predicted by the Curie-Weiss Law when the temperature is decreased further. When the field is applied along the crystallographic *a* axis, the measured susceptibility is stronger than predicted below 60 K for Ol15

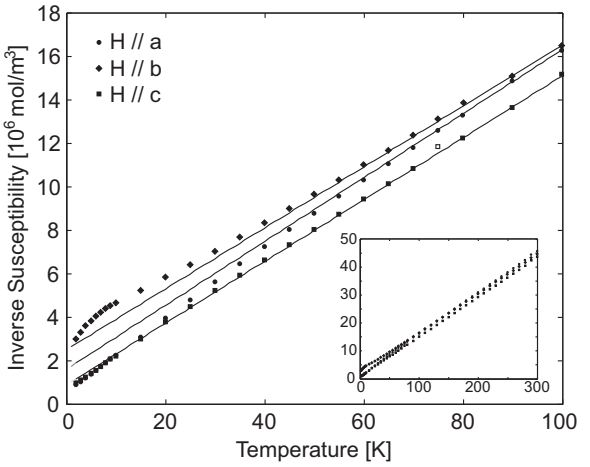

Figure 3. Inverse molar susceptibility along the three crystallographic axes plotted as a function of temperature. Symbols represent the measured data and lines the modeled paramagnetic susceptibility.

or 90 K for Ol14. Only a minor deviation towards higher susceptibility compared to Curie-Weiss behavior can be seen in Ol15 for T < 10 K when the field is parallel to the *c* axis. In relation to the anisotropy measured, the susceptibility along the *a*- and *b*-axes is very similar ($1.84*10^{-8}$ m^3/mol and $1.80*10^{-8}$ m^3/mol for Ol14, and $2.47*10^{-8}$ m^3/mol and $2.38*10^{-8}$ m^3/mol for Ol15) at room temperature. At 77 K the susceptibility parallel to the *b* axis is affected by the onset of local magnetic order and smaller than the susceptibility parallel to *a* (Figure 3).

4.3.2. Low-Field AMS

Most crystals in the Fo90–Fo96 range have mean susceptibility on the order of $1.5* 10^{-7}$ m^3/kg; there is a good agreement with the high-field susceptibility χ_{hf}, on crystals where this was determined. The mean susceptibilities of e.g. NMB45445 and Ol14 are five to 20 times larger than those of the other fresh crystals, which is due to ferrimagnetic inclusions. The weathered crystals have higher mean susceptibilities and show a larger variation. The forsterite crystals Fo1 and Fo2 have very weak susceptibilities and appear diamagnetic when measured on the MFK1 susceptibility bridge but paramagnetic on the VSM, which might be explained by incomplete subtraction of the holder signal, i.e. the glue used to fix the sample within the plastic cylinder was not corrected for in the MFK1 measurement. It cannot be ruled out that the glue also influenced the low-field AMS of forsterite, however, it is not expected that the effect is large given the relative amounts of crystal and glue. All other crystals display mean susceptibilities that are at least an order of magnitude higher than that of forsterite and the effect of the glue is negligible. The low-field AMS of each crystal was measured 10 times, and averaged principal directions are shown for each crystal in Figure 4. The anisotropy is significant for all crystals except Ol11. The maximum susceptibility groups around the crystallographic *c* axis, whereas the intermediate and minimum susceptibilities are distributed in the *a*-*b*-plane. Nearly all crystals have inherent anisotropies between 3% and 10% ($P = k_1/k_3$ 1.03–1.10), except for samples with ferromagnetic contributions, which have a higher degree of anisotropy. This is best illustrated in samples that showed a high saturation remanence, e.g. NMB45445 and Ol14 with $P = 3.03$ and 2.54, respectively. The large *P*-values of the two forsterite crystals are due to their weak susceptibility [cf. *Hrouda*, 2004; *Biedermann et al.*, 2013]. Most samples display a prolate shape of the low-field AMS ellipsoid (supporting information, Table B).

4.3.3. High-Field AMS

Torque measurements in high fields, unlike the low-field measurements, allow for separation of paramagnetic and ferrimagnetic contributions to the AMS. The torque for the forsterite crystals is weak but significant at room temperature. At low temperature, however, the noise level is higher and dominates the torque signal. The principal susceptibilities show different directions for both crystals at room temperature and neither is parallel to the crystallographic axes. AMS directions are not well defined for these crystals

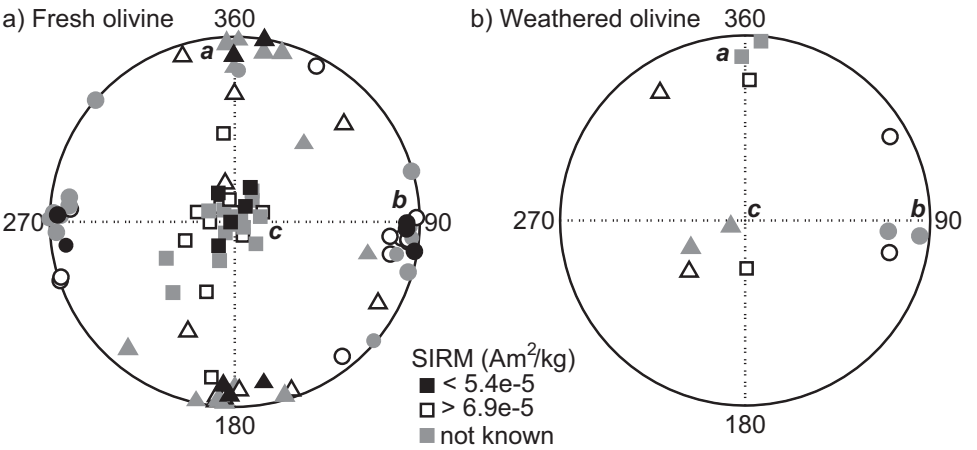

Figure 4. Lower-hemisphere, equal area stereoplots of the low-field AMS of fresh (a), and weathered (b) olivine crystals. Letters indicate crystallographic directions. k_1 are represented by squares, k_2 by triangles, and k_3 by circles for this and subsequent figures.

because the torque response is at the sensitivity level of the torquemeter. This could be due to a superposition of diamagnetic and paramagnetic fabrics, as indicated by the decrease in anisotropy at low temperature. A separation of these two components was not possible.

For most of the crystals with >3 wt % FeO, the paramagnetic component is dominant, and responsible for ca. 90 % of the anisotropy (supporting information, Table C). A typical example of the torque signal is shown in supporting information, Figure A. The anisotropy of one crystal, Ol11, was not significantly above the noise level. For all other samples, the principal paramagnetic susceptibilities are clearly related to crystallographic axes of the olivine crystals (Figure 5). The k_1 axes are aligned along *c* in all fresh olivine crystals. Of these, 10 crystals have 3–5 wt % FeO and 19 samples (18 of which have significant anisotropy) contain 6–10 wt % FeO. For most crystals of the latter group, k_2 is along the *a* axis and k_3 is along the *b* axis at room temperature. For the crystals whose FeO-content is 3–5 wt %, k_3 is dominantly along the crystallographic *a* axis. The degree of anisotropy, k', varies from $3.1*10^{-9}$ m^3/kg to $5.7*10^{-9}$ m^3/kg and the *U*-parameter is prolate for all samples except one and ranges from −0.99 to +0.14. The weathered samples have their maximum paramagnetic susceptibility parallel to the crystallographic *c* axis, and the minimum susceptibility parallel to the *b* axis, similar to the other crystals with higher iron content. However, they have more oblate ellipsoid shapes, with *U* ranging from 0.02 to 0.23.

The paramagnetic anisotropy becomes more dominant at 77 K. The orientation of the k_1 axes does not change significantly in the fresh samples, but the k_2 axes are all oriented about the *a* axis of their respective crystals, and the k_3 axes are grouped around the *b* crystallographic axes (Figure 5). The weathered olivine shows a different behavior at 77 K; while the minimum susceptibility remains parallel to the *b* axis, the maximum is now parallel to the *a* axis. The shape of the AMS ellipsoids is shifted toward the oblate field at low temperature (Figure 6). At 77 K, the fresh olivine exhibits *U*-values between −0.55 and +0.35 and the weathered olivine has *U* between +0.55 and +0.67. The degree of the paramagnetic anisotropy increases with decreasing temperature. This increase can be quantified by p'_{77}, defined as $p'_{77}=k'_{77K}/k'_{298K}$, which is not significantly different from p_{77} defined by *Schmidt et al.* [2007]. The degree of the paramagnetic contribution to the high-field AMS increases at 77 K by an average of 7.1 ± 0.5 with respect to room temperature for fresh olivine and 8.0 ± 0.3 for weathered crystals.

The ferromagnetic component of the anisotropy is weak and usually contributes less than 10 % to the torque signal. Even though the contribution is not significant for most samples, the principal directions of this component are surprisingly consistent, in particular for the crystals with 3–5 wt % FeO, which are mainly from the Sapat Complex, Pakistan. The maximum susceptibility of the ferromagnetic component is tilted 45° with respect to the crystallographic *c* axis of the olivine (Figure 5). The shape parameter *U* covers the entire range from −0.83 to 0.87 and the anisotropy degree of the ferromagnetic AMS varies between $1.3*10^{-10}$ m^3/kg and $2.8*10^{-8}$ m^3/kg (supporting information, Table C).

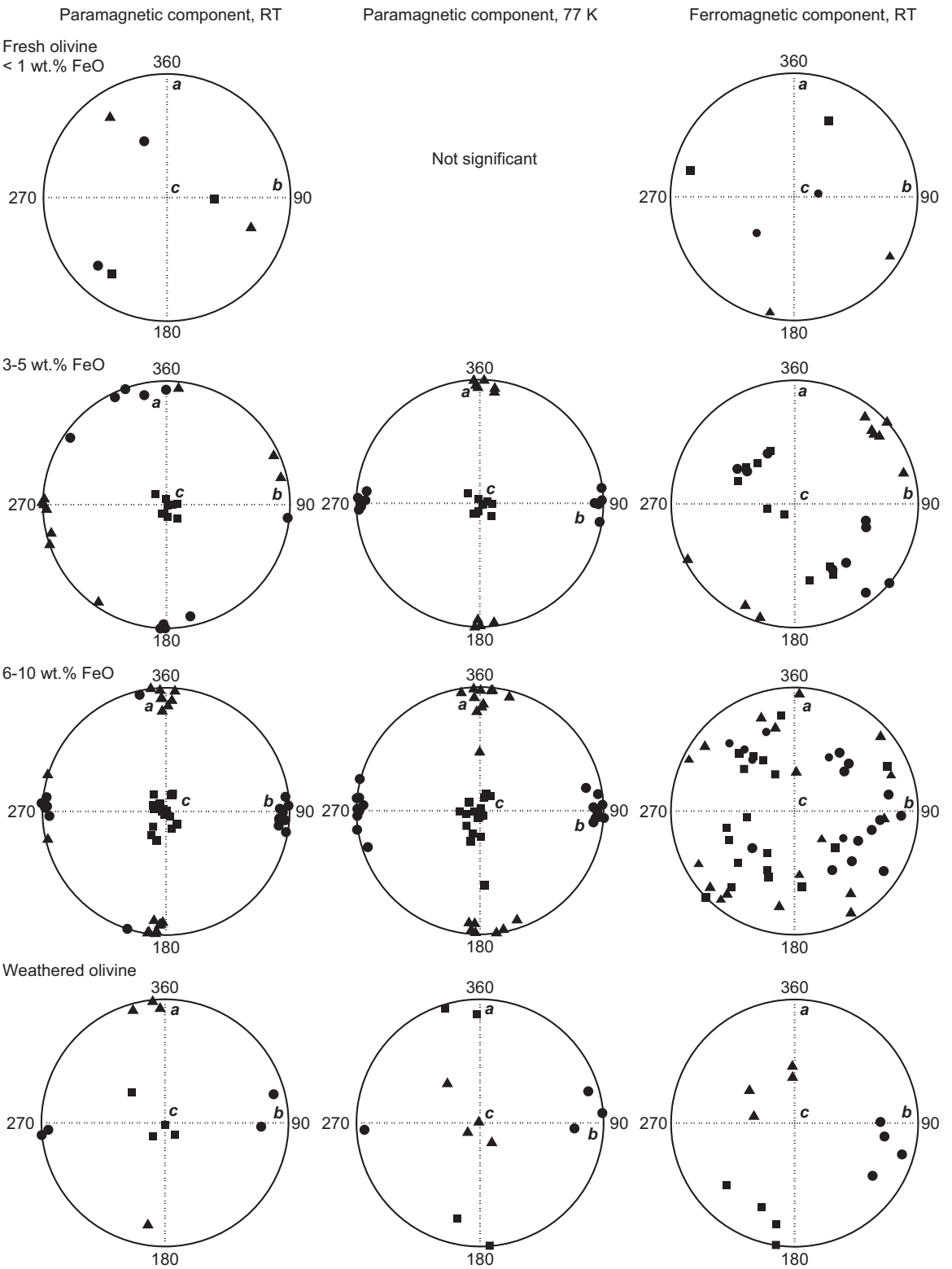

Figure 5. Lower-hemisphere, equal area stereoplots of the paramagnetic, and ferromagnetic principal directions of the high-field AMS for fresh samples with different iron contents and for weathered samples.

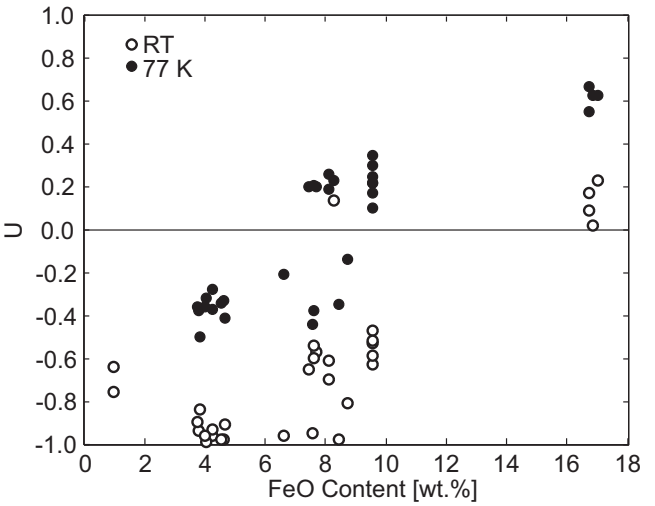

Figure 6. AMS shape *U* as a function of iron content.

5. Discussion

The mean magnetic susceptibility shows a general increase with iron content (Figure 7). Exceptions to this general trend are samples, whose susceptibilities are mainly due to magnetite inclusions, e.g. Ol14 and NMB45445 and the weathered crystals. These crystals displayed SIRM $> 7.1*10^{-4}$ Am^2/kg. Our data agree with the relationship of susceptibility and fayalite content of both *Nagata et al.* [1957] and *Hoye and O'Reilly* [1972], within the limited compositional range.

At T $<$ 100 K, the susceptibility parallel to the crystallographic *b* axis is lower than expected based on the Curie-Weiss law. This can be attributed to the onset of local antiferromagnetic interactions, which agrees with the occurrence of antiferromagnetic ordering in fayalite as described by *Ballet et al.* [1989]. The susceptibility along the *c* axis continues to follow the Curie-Weiss law down to 10 K in Ol15. Similarly, the susceptibility along the *c* axis in fayalite corresponds to a Curie-Weiss behavior below the Néel temperature [*Ballet et al.*, 1989]. It appears that local ferromagnetic ordering may occur along the *a* axis due to canting of the spins, which could result from dipolar interaction, anisotropic exchange coupling, or a weak single ion anisotropy [*Ballet et al.*, 1989; *Ehrenberg and Fuess*, 1993; *Müller et al.*, 1982]. Overall, however, the antiferromagnetic interactions dominate. We found Curie temperatures of -11 K, -18 K and between -4 and -6 K for a magnetic field applied parallel to the crystallographic *a*-, *b*-, and *c*-axes, respectively. *Hoye and O'Reilly* [1972] provided a formula to calculate the Curie temperature, $\theta = -87x$, where *x* is the fayalite mole fraction. In our samples, $x = 0.076$, which leads to $\theta = -6.6\ K$. This lies within the range of directionally dependent temperatures found in our samples. The low-field anisotropy has been shown to be influenced by ferromagnetic inclusions in the crystal. The principal directions of low-field susceptibility lie close to the paramagnetic principal susceptibilities of their respective crystals as long as the SIRM is not larger than $5.4*10^{-5}$ Am^2/kg. Mean susceptibility on the other hand is less affected by the ferromagnetic inclusions until their concentration increases by a factor of 10. Thus, the low-field magnetic anisotropy can be affected by ferromagnetic inclusions in a crystal, where this may not be obvious from the mean susceptibility values.

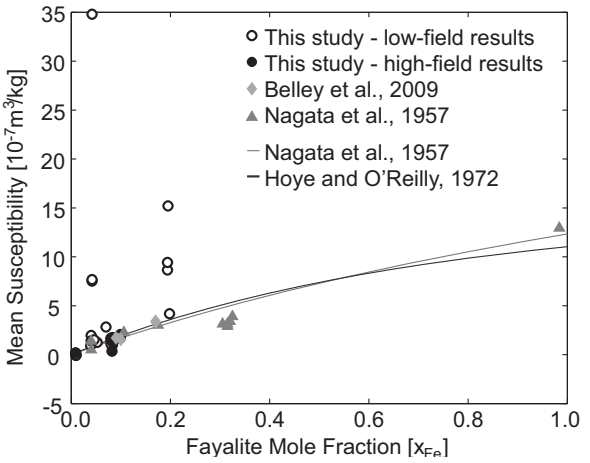

Figure 7. Mean susceptibility as a function of iron content for this and other studies.

Most samples with SIRM $>6.9*10^{-5}$ Am^2/kg display an AMS ellipsoid that is tilted with respect to the pure paramagnetic ellipsoid. Samples with SIRM $>10^{-4}$ Am^2/kg have higher *P*-values than samples that showed purely paramagnetic behavior from their magnetization curves. The saturation remanence of many samples that acquired an IRM indicates that the concentration of magnetite is very low, and does not have a significant contribution to the mean susceptibility. These samples

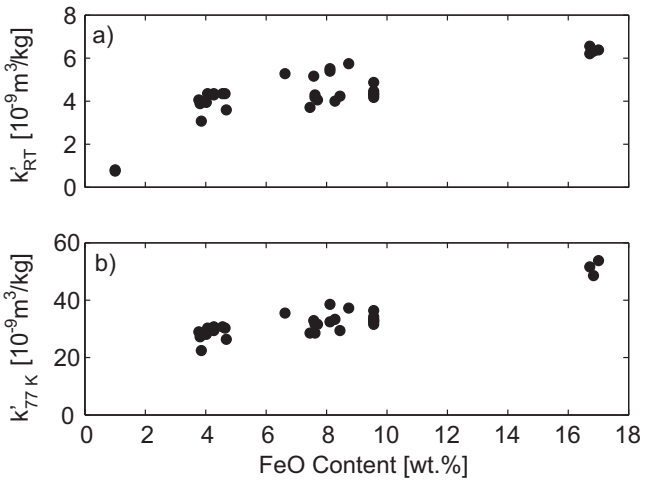

Figure 8. High-field anisotropy degree, k', plotted as a function of Fe-content at room temperature (a) and 77 K (b).

display no relationship between the degree of anisotropy, expressed either as P or k', with iron content (supporting information, Figure B). The higher P-values of the forsterites can be attributed to the low value of mean susceptibility [*Biedermann et al*., 2013; *Hrouda*, 2004].

The paramagnetic component of the high-field AMS is related to the silicate lattice, whereas the ferromagnetic component can be attributed to iron oxide inclusions. Olivine has an orthorhombic crystal structure. According to Neumann's principle [*Neumann*, 1885], any physical property of a crystal must include all symmetry elements of its point group. In the case of an orthorhombic crystal, the principal axes of any second-order tensor property must be parallel to the crystallographic axes.

A significant magnetic anisotropy was only found in the two forsterite crystals when measured at room temperature in high fields, and their principal AMS directions are variable. This could be explained by varying contributions of paramagnetic and diamagnetic effects. The samples become less anisotropic at low temperature, i.e. enhancement of the temperature-dependent paramagnetic contribution is more isotropic. This suggests that the observed anisotropy at room temperature arises from a combination of paramagnetic and diamagnetic contributions or van Vleck paramagnetism.

All crystals containing more than 3 wt % FeO show a clear alignment of the principal susceptibilities with the crystallographic axes. The grouping of paramagnetic principal susceptibilities is better at low temperature, where the paramagnetic anisotropy is enhanced. At low temperature, the minimum susceptibility is parallel to b, whereas it can be parallel to a or b at room temperature, depending on the iron content. Fresh olivine crystals containing $>$6 wt % FeO show a similar relationship in the orientation of the principal axes of paramagnetic anisotropy compared to published experimental and theoretical studies on fayalite—their maximum susceptibility is parallel to the crystallographic c axis, and the minimum susceptibility parallel to the b axis [*Ballet et al*., 1989; *Ehrenberg and Fuess*, 1993]. Thus, their AMS can be explained by the large magnetic moment of iron, which dominates the magnetic signal. Several studies have shown that for solid solutions in the olivine group, iron atoms show a small preference for the M1 sites over the M2 sites [*Deer et al*., 1997 and references therein]. The enrichment of iron in M1 is variable and shows no correlation to bulk composition. The preference of iron for M1 sites, together with the fact that Fe^{2+} on M1 sites results in an easy magnetization direction parallel to the c axis [*Ballet et al*., 1987], explains why the k_1 principal axes of the fresh crystals are parallel to c. In samples with 3–5 wt % FeO, the intermediate and minimum susceptibilities can be interchanged at room temperature. The weathered crystals with FeO $\sim$17 wt % have their minimum susceptibility parallel to b at both temperatures, but the maximum susceptibility switches from c to a at 77 K. The change in AMS principal directions between the fresh and weathered olivine crystals can be attributed to the chemical alteration of olivine to iddingsite, which introduces hydroxyls into the structure. This will affect the interatomic distances or crystal fields, which will in turn influence the magnetic anisotropy.

The shape of the AMS is prolate for the fresh crystals at room temperature and more neutral at 77 K. *Müller et al*. [1982] measured the temperature dependence of susceptibility in fayalite between 4.2 K and 120 K and showed that the susceptibility is different along all three axes at 4.2 K and 35 K, but that the susceptibilities along a and b are the same at 120 K. A similar behavior is presented here for Mg-rich olivine—the susceptibilities parallel to the a- and b-axes are nearly equal at room temperature, but differ at 77 K due to the onset of magnetic ordering below $\sim$100 K. The degree of anisotropy of the paramagnetic AMS increases with iron content, although there is an additional variability in the data (Figure 8). Further, the shape of the

AMS ellipsoid is more prolate for samples with <5 wt % FeO than for those with >6 wt % FeO, and the weathered samples all plot in the oblate field.

A ferromagnetic contribution to the susceptibility and its anisotropy was detected in part of our samples, related to a low-coercivity phase such as magnetite. Although the contribution of the ferromagnetic component of the AMS is weak, its directions are consistent, with the maximum principal susceptibility tilted at 45° to the *c* axis of the host olivine. Several studies have shown that nucleation and growth of inclusions in olivine is controlled crystallographically; e.g. Fe-Ni globules in chondritic olivine grow such that the (110) axis of the metal is parallel to (100) of olivine [*Lappe et al*., 2011; *Leroux et al*., 2003]. We suggest tentatively that similar relationships may hold for magnetite in olivine. Further work is needed, however, to investigate the directional relationship of magnetite inclusions in terrestrial olivine.

Due to the well-defined magnetic anisotropy which is related to the crystallographic lattice of olivine, AMS is a proxy for rock texture in olivine-dominated rocks. Olivine AMS can be used to investigate deformation or flow patterns in the upper mantle. *Hrouda et al*. [2009] provides an example of how the AMS-derived fabric can give insight into processes of emplacement of an ultramafic body. Furthermore, magnetic anisotropy may be used to infer seismic anisotropy in the upper mantle.

If the orientation distribution function of crystals in an olivine-rich rock is known, results for individual single crystals can be used to compute the magnetic anisotropy of the bulk rock. This can be done for (1) the paramagnetic component, given that ferromagnetic inclusions are absent or display random orientation, which would carry no anisotropy, and (2) for the ferromagnetic component if ferromagnetic inclusions are consistently oriented with respect to olivine. This is the case for several crystals used in this study that have a ferromagnetic anisotropy. The ferromagnetic fabric will be dependent on when the ferromagnetic minerals formed. For example, exsolution products are structurally oriented with respect to the host olivine, whereas minerals formed during alteration processes do not necessarily display a preferred orientation [*Deer et al*., 1997; *Haggerty and Baker*, 1967; *Xuexiang et al*., 2009]. With new satellite data coverage from the SWARM mission [e.g., *Friis-Christensen et al*., 2006], detailed information on crustal magnetic anomalies will become available. Our data are central to the proper interpretation of magnetic anomalies over ultramafic bodies, because the paramagnetic and ferromagnetic anisotropies cause a tilt in the magnetization with respect to the magnetic field. In other words, rock texture can deflect magnetization that will thus not be parallel to the ambient magnetic field, but can be tilted toward the magnetic lineation. This anisotropy may have to be taken into consideration when modeling observed magnetic anomalies.

6. Conclusions

The magnetic signal of olivine is dominated by iron. Mg^{2+}, Si^{4+}, and O^{2-} are all diamagnetic whereas Fe^{2+} is paramagnetic and possesses a strong magnetic moment. Pure forsterite should have a negative mean susceptibility and exhibit a purely diamagnetic anisotropy. The forsterite crystals (Fo1, Fo2) contain 1 wt % FeO, which is sufficient to cause a positive susceptibility. The AMS of the forsterite crystals is thus a superposition of diamagnetic and paramagnetic contributions, which explains why the principal susceptibilities are not parallel to the crystallographic axes.

Our study has demonstrated that the principal axes of paramagnetic susceptibility can be directly linked to certain crystallographic axes as soon as >3 wt % FeO are present in an olivine crystal. If the iron content is between 6 and 10 wt % FeO in fresh crystals, the maximum and minimum susceptibilities are parallel to the *c*- and *b*-axes, respectively. For crystals with iron contents between 3 and 5 wt %, the minimum susceptibility is mostly parallel to the *a* axis, while the maximum susceptibility remains along the *c* axis. This is due to the ionic anisotropy of iron in the M1 sites, its preferred location. At room temperature, the AMS ellipsoid is highly prolate, especially for samples with iron contents <5 wt % FeO. Samples with 6–10 wt % FeO display a prolate anisotropy ellipsoid, but with a larger difference between k_2 and k_3 than samples with <5 wt % FeO. At 77 K, the AMS is triaxial for all samples. These results do not agree with the results in *Belley et al*. [2009] or *Ferré et al*. [2005a]. They do agree, however, with *Ferré et al*. [2005b] and with AMS results for fayalite [*Ballet et al*., 1989; *Cococcioni et al*., 2003; *Ehrenberg and Fuess*, 1993; *Müller et al*., 1982]. The degree of high-field anisotropy increases by a factor (p'_{77}) of 7.1 ± 0.5 at 77 K compared to room temperature. The different behavior displayed by the weathered crystals highlights how differences in mineral composition can affect the AMS. Our findings

have great potential for using AMS as a proxy for mantle deformation. They also have implications for modeling magnetic anomalies observed over deformed ultramafic rock domains.

Acknowledgments
P. Bouilhol, Durham University, A. Puschnig, Natural History Museum Basel, P. Brack & M. Schmidt, ETH Zurich, and the Swiss Gemmological Institute—SSEF kindly provided samples for this study. W.E.A Lorenz is thanked for help with the low-temperature measurements. We are grateful to Eric Ferré and Mike Jackson for their constructive reviews. This study was funded by the Swiss National Science Foundation, projects 200021_129806 and 200020_143438.

References

Ballet, O., H. Fuess, and T. Fritzsche (1987), Magnetic structure and cation distribution in $(Fe,Mn)_2SiO_4$ (Olivine) by neutron diffraction, *Phys. Chem. Miner.*, *15*, 54–58.

Ballet, O., H. Fuess, K. Wacker, E. Untersteller, W. Treutmann, E. Hellner, and S. Hosoya (1989), Magnetisation measurements of the synthetic olivine single crystals A_2SiO_4 with A = Mn, Fe or Co, *J. Phys. Conden. Matter*, *1*, 4955–4970.

Belley, F., E. C. Ferré, F. Martín-Hernández, M. J. Jackson, M. D. Dyar, and E. J. Catlos (2009), The magnetic properties of natural and synthetic $(Fe_x, Mg_{1-x})_2$ SiO_4 olivines, *Earth Planet. Sci. Lett.*, *284*, 516–526, doi:10.1016/j.epsl.2009.05.016.

Bergmüller, F., C. Bärlocher, B. Geyer, M. Grieder, F. Heller, and P. Zweifel (1994), A torque magnetometer for measurements of the high-field anisotropy of rocks and crystals, *Meas. Sci. Technol.*, *5*, 1466–1470.

Biedermann, A. R., W. Lowrie, and A. M. Hirt (2013), A method for improving the measurement of low-field magnetic susceptibility anisotropy in weak samples, *J. Appl. Geophys.*, *88*, 122–130, doi:10.1016/j.jappgeo.2012.10.008.

Bouilhol, P., J.-P. Burg, J.-L. Bodinier, M. W. Schmidt, H. Dawood, and S. Hussain (2009), Magma and fluid percolation in arc to forearc mantle: Evidence from Sapat (Kohistan, Northern Pakistan), *Lithos*, *107*, 17–37, doi:10.1016/j.lithos.2008.07.004.

Bouilhol, P., J. P. Burg, J. L. Bodinier, M. W. Schmidt, S. M. Bernasconi, and H. Dawood (2012), Gem olivine and calcite mineralization precipitated from subduction-derived fluids in the Kohistan Arc-Mantle (Pakistan), *Can. Mineral.*, *50*, 1291–1304, doi:10.3749/canmin.50.5.1291.

Chen, S. H., S. Y. O'Reilly, X. H. Zhou, W. L. Griffin, G. H. Zhang, M. Sun, J. L. Feng, and M. Zhang (2001), Thermal and petrological structure of the lithosphere beneath Hannuoba, Sino-Korean Craton, China: Evidence from xenoliths, *Lithos*, *56*, 267–301.

Cococcioni, M., A. Dal Corso, and S. de Gironcoli (2003), Structural, electronic, and magnetic properties of Fe_2SiO_4 fayalite: Comparison of LDA and GGA results, *Phys. Rev. B*, *67*, 094106, doi:10.1103/PhysRevB.67.094106.

Deer, W. A., R. A. Howie, and J. Zussman (1997), *Orthosilicates*, 2nd ed., Geol. Soc., London, U. K.

Ehrenberg, H., and H. Fuess (1993), Analytical interpretation and simulation of the static magnetic properties of synthetic alpha-Fe_2SiO_4, *J. Phys. Conden. Matter*, *5*, 3663–3672.

Ferré, E. C., B. Tikoff, and M. Jackson (2005a), Corrigendum to "The magnetic anisotropy of mantle peridotites: Example from the Twin Sisters dunite, Washington", [*Tectonophysics 398* (2005) 141–166], *Tectonophysics*, *405*, 233, doi:10.1016/j.tecto.2005.06.001.

Ferré, E. C., B. Tikoff, and M. Jackson (2005b), The magnetic anisotropy of mantle peridotites: Example from the Twin Sisters dunite, Washington, *Tectonophysics*, *398*, 141–166, doi:10.1016/j.tecto.2005.02.001.

Friis-Christensen, E., H. Luhr, and G. Hulot (2006), Swarm: A constellation to study the Earth's magnetic field, *Earth Planets Space*, *58*, 351–358.

Guillong, M., D. L. Meier, M. M. Allan, C. A. Heinrich, and B. W. D. Yardley (2008), SILLS: A MATLAB-based program for the reduction of laser ablation ICP-MS data of homogeneous materials and inclusions, *Miner. Assoc. Can. Short Course*, *40*, 328–333.

Haggerty, S. E., and I. Baker (1967), The alteration of olivine in basaltiv and associated lavas. Part I: High temperature alteration, *Contrib. Mineral. Petrol.*, *16*, 233–257.

Hoffmann, V. H., R. Hochleitner, M. Torii, M. Funaki, T. Mikouchi, M. Kaliwoda, P. Jenniskens, and M. H. Shaddad (2011), Magnetism and mineralogy of Almahata Sitta polymict ureilite (= asteroid 2008 TC3): Implications for the ureilite parent body magnetic field, *Meteorit. Planet. Sci.*, *46*, 1551–1564, doi:10.1111/j.1945-5100.2011.01248.x.

Hoye, G. S., and W. O'Reilly (1972), A magnetic study of the ferro-magnesian olivines $(Fe_xMg_{1-x})SiO_4$, $0 < x < 1$, *J. Phys. Chem. Solids*, *33*, 1827–1834.

Hrouda, F. (1982), Magnetic anisotropy of rocks and its application in geology and geophysics, *Geophys. Surv.*, *5*, 37–82.

Hrouda, F. (2004), Problems in interpreting AMS parameters in diamagnetic rocks, in *Magnetic Fabric: Methods and Applications*, edited by F. Martín-Hernández, et al., pp. 49–59, Geol. Soc., London, U. K.

Hrouda, F., S. W. Faryad, P. Jeřábek, M. Chlupáčová, and P. Vitouš (2009), Primary magnetic fabric in an ultramafic body (Moldanubian Zone, European Variscides) survives exhumation-related granulite-amphibolite facies metamorphism, *Lithos*, *111*, 95–111, doi:10.1016/j.lithos.2008.10.004.

Jarosewich, E., J. A. Nelen, and J. A. Norberg (1980), Reference samples for electron microprobe analysis, *Geostand. Newsl.*, *4*, 43–47.

Jelinek, V. (1981), Characterization of the magnetic fabric of rocks, *Tectonophysics*, *79*, T63–T67.

Jelinek, V. (1984), On a mixed quadratic invariant of the magnetic susceptibility tensor, *J. Geophys.*, *56*, 58–60.

Kane, R. E. (2004), The creation of a magnificent suite of peridot jewelry: From the Himalayas to Fifth Avenue, *Gems Gemol.*, *40*, 288–302.

Kurat, G., H. Palme, A. Embey-Isztin, J. Touret, T. Ntaflos, B. Spettel, F. Brandstätter, C. Palme, G. Dreibus, and M. Prinz (1993), Petrology and geochemistry of peridotites and associated vein rocks of Zabargad Island, Red Sea, Egypt, *Mineral. Petrol.*, *48*, 309–341.

Lappe, S.-C., N. S. Church, T. Kasama, A. Bastos da Silva Fanta, G. Bromiley, R. E. Dunin-Borkowski, J. M. Feinberg, S. Russell, and R. J. Harrison (2011), Mineral magnetism of dusty olivine: A credible recorder of pre-accretionary remanence, *Geochem. Geophys. Geosyst.*, *12*, Q12Z35, doi:10.1029/2011GC003811.

Laugier, J., and A. Filhol (1983), An interactive program for the interpretation and simulation of Laue patterns, *J. Appl. Crystallogr.*, *16*, 281–283.

Leroux, H., G. Libourel, L. Lemelle, and F. Guyot (2003), Experimental study and TEM characterization of dusty olivines in chondrites: Evidence for formation by in situ reduction, *Meteorit. Planet. Sci.*, *38*, 81–94, doi:10.1111/j.1945-5100.2003.tb01047.x.

Martín-Hernández, F., and A. M. Hirt (2001), Separation of ferrimagnetic and paramagnetic anisotropies using a high-field torsion magnetometer, *Tectonophysics*, *337*, 209–221, doi:10.1016/s0040-1951(01)00116-0.

Martín-Hernández, F., and A. M. Hirt (2004), A method for the separation of paramagnetic, ferrimagnetic and haematite magnetic subfabrics using high-field torque magnetometry, *Geophys. J. Int.*, *157*, 117–127, doi: 10.1111/j.1365-246X.2004.02225.x.

Müller, R., H. Fuess, and P. J. Brown (1982), Magnetic properties of synthetic fayalite (α-Fe2SiO4), *Le Journal de Physique Colloques*, *43*, C7-249–C247–252.

Nagata, T., T. Yukutake, and S. Uyeda (1957), On magnetic susceptibility of olivines, *J. Geomagn. Geoelectr.*, *9*, 51–56.

Neumann, F. E. (1885), Vorlesungen über die Theorie der Elastizität der Festen Körper und des Lichtäthers, B.G. Teubner Verlag, Leipzig, Germany.

Nicolas, A., and N. I. Christensen (1987), Formation of anisotropy in upper mantle peridotites: A review, in *Composition, Structure and Dynamics of the Lithosphere-Asthenosphere System*, edited by K. Fuchs and C. Froidevaux, pp. 111–123, *Geodyn. Ser. AGU*, Washington, D. C.

Owens, W. H., and D. Bamford (1976), Magnetic, seismic, and other anisotropic properties of rock fabrics, *Philos. Trans. R. Soc. A*, *283*, 55–68.

Pettke, T., F. Oberli, A. Audetat, M. Guillong, A. Simon, J. Hanley, and L. M. Klemm (2012), Recent developments in element concentration and isotope ratio analysis of individual fluid inclusions by laser ablation single and multiple collector ICP–MS, *Ore. Geol. Rev.*, *44*, 10–38, doi:10.1016/j.oregeorev.2011.11.001.

Rochette, P., B. P. Weiss, and J. Gattacceca (2009), Magnetism of extraterrestrial materials, *Elements*, *5*, 223–228, doi:10.2113/gselements.5.4.223.

Rudnick, R. L., G. Shan, W. L. Ling, Y. S. Liu, and W. F. McDonough (2004), Petrology and geochemistry of spinel peridotite xenoliths from Hannuoba and Qixia, North China craton, *Lithos*, *77*, 609–637, doi:10.1016/j.lithos.2004.03.033.

Schmidt, V., A. M. Hirt, P. Rosselli, and F. Martín-Hernández (2007), Separation of diamagnetic and paramagnetic anisotropy by high-field, low-temperature torque measurements, *Geophys. J. Int.*, *168*, 40–47, doi:10.1111/j.1365-246X.2006.03202.x.

Silver, P.G. (1996), Seismic anisotropy beneath the continents: Probing the depths of geology, *Annu. Rev. Earth Planet. Sci.*, *24*, 385–432.

Tommasi, A., M. Knoll, A. Vauchez, J. W. Signorelli, C. Thoraval, and R. Logé (2009), Structural reactivation in plate tectonics controlled by olivine crystal anisotropy, *Nat. Geosci.*, *2*, 423–427, doi:10.1038/ngeo528.

Uehara, M., and N. Nakamura (2006), Experimental constraints on magnetic stability of chondrules and the paleomagnetic significance of dusty olivines, *Earth Planet. Sci. Lett.*, *250*, 292–305, doi:10.1016/j.epsl.2006.07.042.

Xuexiang, Q., J. C. Grimmer, and X. Zhiqin (2009), Ultrahigh-pressure texture inheritance during retrogression: Evidence from magnetofabrics in eclogites and ultramafic rocks (Chinese Continental Scientific Drilling project), *Tectonophysics*, *475*, 267–278, doi: 10.1016/j.tecto.2008.09.015.